Iron Bound to the High-Affinity Mn-Binding Site of the Oxygen-Evolving Complex Shifts the p*K* of a Component Controlling Electron Transport via Y_Z[†]

Boris K. Semin[‡,§] and Michael Seibert*[,‡]

Basic Sciences Center, National Renewable Energy Laboratory, Golden, Colorado 80401, and Department of Biophysics, Faculty of Biology, Moscow State University, Moscow 119899, Russian Federation

Received November 15, 2003; Revised Manuscript Received March 23, 2004

ABSTRACT: Flash-probe fluorescence spectroscopy was used to compare the pH dependence of charge recombination between $Y_Z^{\bullet}$ and Q_a^- in Mn-depleted, photosystem II membranes [PSII(−Mn)] and in membranes with the high-affinity (HA_Z) Mn-binding site blocked by iron [PSII(−Mn,+Fe); Semin, B. K., Ghirardi, M. L., and Seibert, M. (2002) *Biochemistry 41*, 5854−5864]. The apparent half-time for fluorescence decay ($t_{1/2}$) in PSII(−Mn) increased from 9 ms at pH 4.4 to 75 ms at pH 9.0 [with an apparent p*K* (pK_{app}) of 7.1]. The actual fluorescence decay kinetics can be fit to one exponential component at pH <6.0 ($t_{1/2}$ = 9.5 ms), but it requires an additional component at pH >6.0 ($t_{1/2}$ = 385 ms). Similar measurements with PSII(−Mn,+Fe) membranes show that iron binding has little effect on the maximum and minimum $t_{1/2}$ values measured at alkaline and acidic pHs but that it does shift the pK_{app} from 7.1 to 6.1 toward the more acidic pK_{app} value typical of intact membranes. Light-induced Fe(II) blocking of the PSII(−Mn) membrane is accompanied by a decrease in buffer Fe(II) concentration. This decrease was not the result of Fe(II) binding, but rather of its oxidation at two sites, the HA_Z site and the low-affinity site. Mössbauer spectroscopy at 80 K on PSII(−Mn,+Fe) samples, prepared under conditions providing the maximal blocking effect but minimizing the amount of nonspecifically bound iron cations, supports this conclusion since this method detected only Fe(III) cations bound to the membranes. Correlation of the kinetics of Fe(II) oxidation with the blocking parameters showed that blocking occurs after four to five Fe(II) cations were oxidized at the HA_Z site. In summary, the blocking of the HA_Z Mn-binding site by iron in PSII(−Mn) membranes not only prevents the access of exogenous donors to Y_Z but also partially restores the properties of the hydrogen bond net found in intact PS(II), which in turn controls the rate of electron transport to Y_Z.

The catalytic center of the oxygen-evolving complex (OEC)[1] of photosystem II (PSII) consists of four Mn ions (the tetrameric Mn cluster), parts of the D1 polypeptide, one Ca cation, and one or two chloride anions. This ensemble can accumulate four oxidizing equivalents that are used to oxidize two water molecules and release molecular O_2. The water oxidation process is initiated by light-driven excitation of the primary electron donor, P680, which results in the formation of the charge-separated state, $P680^+Q_a^-$. Oxidized P680 is a strong oxidant (E_m = 1.1 V) (*1*), which oxidizes the redox-active tyrozine Y_Z (D1-Y161) within tens of nanoseconds (*2*−*4*) and generates $Y_Z^{\bullet}$, the neutral form of the radical (*5*−*7*). This radical in turn oxidizes the OEC with a rate that depends on the S-state of the Mn cluster, i.e., from tens of microseconds during the S1 → S2 transition to 1.2−1.4 ms during the S3 → S0 transition (*8*).

Recent results show that the distance between Y_Z and the Mn cluster is 7−9 Å (*9*−*11*). Such a short distance allows for the formation of a hydrogen bond either directly between the phenol oxygen of Y_Z and a Mn-bound substrate water molecule (*8*, *12*) or indirectly via an intervening water molecule (*13*). These observations form the basis of new models for water oxidation in PSII, in which Y_Z is a part of the OEC and thus participates directly in water photochemistry. According to these models, Y_Z extracts either protons (*14*) or hydrogen atoms (*15*, *16*) from water molecules coordinated to Mn. In turn, the oxidation of Y_Z by $P680^+$ is accompanied by the release of a phenolic proton from Y_Z and the formation of a neutral tyrosine radical on Y_Z.

This proposed mechanism for electron and proton transfer through Y_Z requires the presence of another species [base B

[†] This work was sponsored by the NREL Director's Discretionary Research and Development fund (M.S. and B.K.S.) and by the Division of Energy Biosciences, Office of Science, U.S. Department of Energy (M.S.).

* To whom correspondence should be addressed. Telephone: (303) 384-6279. Fax: (303) 384-6150. E-mail: mike_seibert@nrel.gov.

[‡] National Renewable Energy Laboratory.

[§] Moscow State University.

[1] Abbreviations: Chl, chlorophyll; DCMU, 3-(3,4-dichlorophenyl)-1,1-dimethylurea; DPC, 1,5-diphenylcarbazide; F_0, fluorescence emitted by a sample at low light levels prior to flash excitation; $(F - F_0)/F_0$, fluorescence yield; F_{fin}, final fluorescence yield detected after decay of the flash-induced F_{max}; F_{max}, maximum fluorescence yield following actinic flash excitation; HA_Z, site of high-affinity electron donation to $Y_Z^{\bullet}$ by exogenous donors; MES, 2-(*N*-morpholino)ethanesulfonic acid; OEC, oxygen-evolving complex; P680, primary electron donor in PSII; pK_{app}, apparent p*K*; PSII, photosystem II; PSII(−Mn), Mn-depleted PSII membranes; PSII(−Mn,+Fe), Fe-blocked PSII(−Mn); Q_a, primary quinone acceptor of PSII; Q_b, secondary quinone acceptor of PSII; RC, reaction center; Tris, tris(hydroxymethyl)aminomethane; Y_Z (D1-Tyr161), redox active tyrosine, the first electron donor to $P680^+$ in PSII; Y_D, redox active tyrosine (D2-Tyr160), an alternative electron donor to $P680^+$ in PSII.

10.1021/bi036047p CCC: $27.50
Published on Web 05/05/2004

(*4*)] to accept the proton from Y_Z. A number of studies have shown that tyrozine Y_Z, like tyrozine Y_D, is hydrogen-bonded, but the hydrogen bonds to Y_Z are less ordered than those to Y_D at least in Mn-depleted PSII (*17*−*20*). However, the specific amino acid residue forming the hydrogen bond with Y_Z is yet to be identified conclusively. Computer modeling studies, site-directed mutagenesis, and chemical complementation studies suggest that this role could be performed by D1-His190 (*21*−*26*). This histidine possibly controls not only the rate of Y_Z oxidation but also the rate of $Y_Z^{\bullet}$ reduction by recombination with Q_a^- (*24*). Manganese extraction alters the interaction between Y_Z and base B, and the oxidation of Y_Z becomes rate-limited by its deprotonation (for reviews, see refs *27* and *28*). It has been proposed that this effect is caused by the disruption of the hydrogen bond between Y_Z and His190 (*26*) or by a shift in the pK_{app} of base B (*4*).

In functional PSII membranes, the protein matrix and the presence of the Mn cluster on the donor side prevent the oxidation of exogenous electron donors by redox-active Y_Z and facilitate the high rate (on the time scale of nanoseconds) of electron transfer from Y_Z to $P680^+$. Extraction of Mn, which normally also removes Ca^{2+}, alters the protein environment around Y_Z. As a consequence, Y_Z becomes accessible to the exogenous reductant, Mn(II) (*29*), and an almost 1000-fold decrease in the electron transfer rate between $Y_Z^{\bullet}$ and $P680^+$ results at neutral pH (*4*, *19*, *25*, *26*, *30*, *31*). Extraction of the Mn cluster from PSII is also accompanied by the appearance of the high-affinity (HA_Z), Mn-binding site on the donor side (*32*−*44*). This site specifically binds one Mn cation that is oxidized by $Y_Z^{\bullet}$ (*36*, *42*). Exogenous Mn(II) donates electrons to $Y_Z^{\bullet}$ via this site, which is also thought to bind the first Mn involved in the assembly of the Mn cluster during the photoactivation process. The DPC inhibition assay (*33*−*36*, *38*, *40*, *41*, *45*), EPR (*39*, *42*), optical spectroscopy (*37*), and measurements of flash-probe fluorescence decay (*32*, *38*, *40*−*42*) have all been used to investigate this site. Site-directed mutant (*37*, *43*) and chemical modification (*35*, *36*, *39*, *40*, *44*) studies suggest the involvement of carboxylic groups, probably from D1-Asp170 among others, in the ligation of the Mn cation at this site. Finally, spectroscopic evidence (dual-mode EPR) for Mn(III) formation by the photooxidation of Mn(II) bound at the HA_Z Mn site has been obtained recently (*43*).

A number of different divalent metal cations can interact with the HA_Z site but significantly less efficiently (*35*, *38*) than Mn(II). The DPC inhibition assay has shown that only Fe(II) binds to the HA_Z Mn-binding site as well as Mn(II), and many binding characteristics for both cations are similar (*46*). Kinetic studies have revealed competitive binding of Fe(II) and Mn(II) cations at this site (*47*). The molecular basis for the similarity in binding of the two ions might be explained in terms of the carboxyl ends of the D1 and D2 polypeptides. These constituents of the PSII reaction center contain conservative motifs, which can coordinate either Mn or Fe cations (*48*).

Investigation of the interaction of Fe(II) with the HA_Z site by flash-probe fluorescence has shown that a short preincubation of Mn-depleted PSII membranes under weak light with Fe(II) (conditions resembling those for photoactivation of the Mn cluster) leads to the irreversible binding of more than one Fe cation at the HA_Z Mn donation site (*49*). These bound iron cations inhibit the donation of an electron to $Y_Z^{\bullet}$ by exogenous donors such as Mn(II), Fe(II), and DPC (but not hydroxylamine) (*49*). These results showed that iron bound to the HA_Z site reconstitutes two of the main features of the intact OEC in PSII: the inaccessibility of Y_Z for exogenous electron donors and a stable intermediary metal complex. These two characteristics are also associated with the two-Mn intermediate of the normal photoactivation process. Since the stable binding of iron to the HA_Z site changes the protein environment around Y_Z, we investigated the influence of bound iron on the rate of electron transfer to $Y_Z^{\bullet}$ (i.e., the reduction of $Y_Z^{\bullet}$ by charge recombination) in the current study. As expected, iron binding had a significant effect on the pH dependence of the recombination kinetics compared to that in "unblocked" Mn-depleted PSII membranes.

MATERIALS AND METHODS

Biological Samples. BBY-type, PSII-enriched membrane fragments were prepared from market spinach (*49*) and resuspended in buffer A [50 mM MES/NaOH buffer (pH 6.5), 15 mM NaCl, and 0.4 M sucrose]. Chlorophyll concentrations and Chl *a*/*b* ratios were determined in 80% acetone, according to the method of Porra *et al*. (*50*). The rate of oxygen evolution by the PSII membranes was 400−500 μmol of O_2 (mg of Chl)$^{-1}$ h^{-1}, and the membranes were stored under liquid nitrogen until use. Manganese depletion was accomplished by incubating thawed PSII membranes (0.5 mg of Chl/mL) in 1 M Tris-HCl buffer (pH 9.4), containing 0.4 M sucrose, for 30 min at 5 °C in room light (*35*). Hereafter, these will be termed PSII(−Mn) membranes.

Manganese and Iron Solutions. Concentrated stocks of 0.5 mM $MnCl_2$ and 0.5 mM $FeSO_4$ in double-distilled water were made up just prior to the experiments. Little oxidation of Fe(II) in the stock solution (pH 5.6) was observed after 5 h at room temperature. In contrast, the stability of Fe(II) decreased in buffer A (pH 6.5), but only ∼5% of the Fe(II) was oxidized after a 1 h incubation (*49*).

pH Measurements. The effects of pH on flash-probe fluorescence yield decay kinetics in PSII(−Mn) membranes were examined using MES buffer (50 mM MES/NaOH, 15 mM NaCl, and 0.4 M sucrose) in the pH range of 4.4−6.5 and Tricine buffer (50 mM Tricine, 15 mM NaCl, and 0.4 M sucrose) in the pH range of 7.0−9.0. No differences in the apparent decay kinetics of the samples in MES or Tricine buffers poised at the same pH (pH 7.0) were observed. The pH dependence of the fluorescence decay kinetics in PSII(−Mn,+Fe) membranes (containing an iron-blocked HA_Z Mn-binding site) was measured in MES/NaOH buffer at all pHs below ca. 8.2. Tricine was not used because it can extract iron cations bound to the HA_Z site (*49*, see also Results section below). The pHs of the samples, resuspended in MES buffer outside its optimal buffering capacity (i.e., pH <5.5 or >7.0), were confirmed after addition of all reaction components. At high alkaline pHs (8−13), the fluorescence decay kinetics in PSII(−Mn) membranes were measured in pyrophosphate buffer (20 mM pyrophosphate, 400 mM sucrose, and 15 mM NaCl).

Blocking of the HA_Z Mn-Binding Site. PSII(−Mn,+Fe) membranes were prepared as follows. Mn-depleted PSII membranes (37 μg of Chl/mL) were incubated in buffer A

(pH 6.5) with 7.5 μM Fe(II) under cool white fluorescent room light (4 μE m^{-2} s^{-1}, PAR) for 2 min at room temperature, pelleted by centrifugation, and resuspended in MES buffer (50 mM MES, 0.4 M sucrose, and 15 mM NaCl) at the indicated pH (*49*).

Assessment of Fe(II) Oxidation. The concentration of Fe(II) in buffer A before and after incubation with PSII(−Mn) membranes (following removal of the membranes by centrifugation) was determined utilizing the *o*-phenanthroline procedure by measuring the absorbance of the red-colored ferrous phenanthrolinate complex ($\epsilon_{512} = 11.1$ mM^{-1}) (*49*). The spectroscopic measurements were performed with a Varian Cary 5E spectrophotometer (sensitivity, ±0.002 A; ±0.1 μM Fe).

Flash-Probe Fluorescence Measurements. The decay of the flash-probe fluorescence decay yield was measured at room temperature using a home-built instrument capable of a time resolution of 100 μs (*38*, *49*). Samples, containing 25 μg of Chl/mL (ca. 0.12 μM PSII centers) and 37.5 μM DCMU in buffer A, were adapted to the dark prior to the measurement. Data analysis used Data Translation Global Lab software and a DT2839 A/D board mounted in an ALR 486 personal computer (*38*). The half-times reported in Figures 2 and 6 were the time points at which the fluorescence emission decayed to one-half the maximum value and are termed apparent half-times. The amplitudes of the exponential components, which constitute the actual fluorescence decay kinetics, are shown in Figures 4 and 7. The decay kinetics were approximated by a single-exponential component in the pH region from 4.4 to 6.0 using the equation $y = y_0 + ae^{-bt}$. At higher pHs, two components provided a better fit, and they were obtained using the equation $y = y_0 + ae^{-bt} + ce^{-dt}$.

Mössbauer Spectroscopy. Mn-depleted PSII membranes (15 μg of Chl/mL) were adapted to the dark for 1 h and then incubated at 5 °C in buffer A′ [15 mM MES (pH 6.1), 15 mM NaCl, and 0.4 M sucrose] with 1.5 μM ^{57}Fe(II) for 40 s or 1.0 μM ^{57}Fe(III) for 5 min in cuvettes illuminated as described before except the intensity was ∼40 μE m^{-2} s^{-1}. The membranes were then centrifuged for 25 min at 26000*g*; the pellet was resuspended in the dark in a small volume of buffer A′, and the suspension was centrifuged for 1 h at 100000*g*. The membranes were then transferred to a 0.4 mL Mössbauer cell (20 mg of Chl) and frozen in liquid nitrogen. The Mössbauer spectra were obtained at 80 K using a ^{57}CoRh source. The isomer shifts are given relative to metallic iron at room temperature.

RESULTS

pH Dependence of the Flash-Induced Fluorescence Decay in Mn-Depleted PSII Membranes

pH 4.4−9.0. We first studied the pH dependence of the flash-probe fluorescence decay kinetics in PSII(−Mn) membranes over the range of 4.4−9.0 (Figure 1) and observed the following results. (a) F_{max} increased between pH 5.0 and 7.0, but by a factor of only ∼1.5. (b) F_{fin} started to increase above pH 6.0 but did not reach saturation in the pH range that was investigated. (c) The apparent $t_{1/2}$ (due to charge recombination between Q_a^- and $Y_Z^\bullet$) increased between pH 6.0 and 7.5 (with a pK_{app} of 7.1), but it did not increase further at pH ≥7.5. The pH dependencies of F_{max}, F_{fin}, and the apparent $t_{1/2}$ are presented graphically in Figure 2. The $t_{1/2}$ has a well-defined pH dependence, which suggests the involvement of a protonateable group with a pK_{app} of 7.1 [the pH at which the apparent $t_{1/2} = (t_{1/2}^{max} + t_{1/2}^{min})/2$] in the control of electron transport via Y_Z. The apparent $t_{1/2}^{min}$ that we observe at acidic pHs is ∼9 ms (Figure 2), and this corresponds well with the $t_{1/2}$ value (9.3 ms) found by Mamedov *et al*. (*24*) for thylakoid membranes, isolated from WT *Chlamydomonas reinhardtii* (which do not contain a functional OEC) grown in the dark. In contrast, the apparent

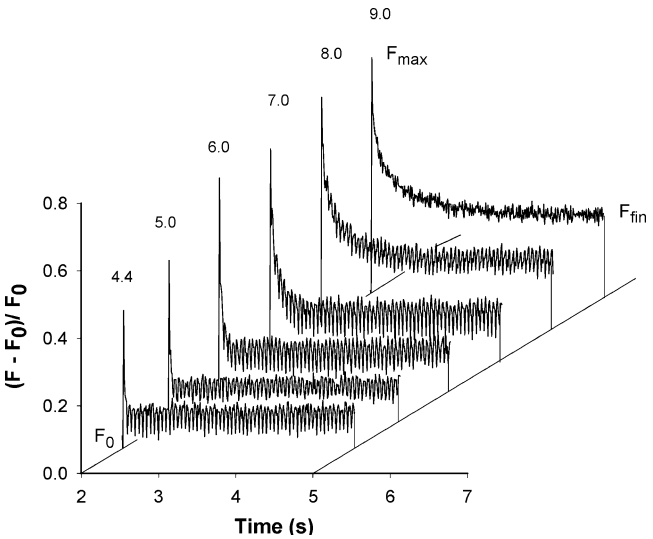

FIGURE 1: Effect of pH on the kinetics of flash-probe Chl fluorescence decay attributed to charge recombination in PSII. Tris-washed (Mn-depleted) spinach PSII membrane fragments [PSII(−Mn)] at 25 μg of Chl/mL were excited with a single-turnover flash. In the way of background information, the Chl *a* fluorescence yield in PSII is governed by the redox states of P680 and Q_a, and it depends on the concentration of reduced primary quinone acceptor Q_a^- that is generated by an excitation flash (*51*) (see the Discussion for comments on the linearity between the fluorescence yield and Q_a^- concentration). The initial dark redox state of the PSII reaction center is P680PheoQ_a, where F_0 is the fluorescence emitted by the samples prior to flash excitation. Light-induced excitation of P680 drives primary electron transfer from P680* to the nearby Pheo primary acceptor, and this transient charge separation is stabilized within 300 ps by the reduction of Q_a by Pheo$^-$ (*52*). Despite the presence of Q_a^-, P680$^+$PheoQ_a^- is still in a low-fluorescence state (F_0) because P680$^+$ is a fluorescence quencher (*53*). Subsequent reduction of P680$^+$ by Y_Z results in the appearance of the high-fluorescence state, $Y_Z^\bullet$P680PheoQ_a^-, and the fluorescence yield increases to the maximum level (F_{max}). Subsequently, Q_a^- can be reoxidized (a) by the secondary quinone acceptor, Q_b, with kinetics of a few hundred microseconds (*54*) or (b) by charge recombination with the tetrameric Mn cluster of the OEC (in intact PSII membranes) or with $Y_Z^\bullet$ (in Mn-depleted PSII). Pathway b occurs in the presence of DCMU, an inhibitor of Q_b reduction by Q_a^-. The subsequent recombination process is accompanied by a decrease in the Q_a^- concentration, which can be monitored from the decay of the fluorescence yield after a saturating flash. The fluorescence reaches a steady state level (F_{fin}) that is higher than F_0 after several tens of milliseconds (*24*, *38*). This observation indicates that some fraction of the Q_a^- pool does not recombine with $Y_Z^\bullet$. It is thought that F_{fin} is governed by the presence of an endogenous electron donor for $Y_Z^\bullet$ of an unknown nature that reduces part of the $Y_Z^\bullet$ population in a sample and as such prevents the total reoxidation of Q_a^- during the recombination process with $Y_Z^\bullet$ (*24*, *55*). In this figure, each sample contained 37.5 μM DCMU. The samples were adapted to the dark for 2 min prior to the measurement. $(F - F_0)/F_0$ is the fluorescence emission normalized to F_0. The numbers in the figure are the pHs of the samples at the time of the experiment. See the text for other experimental conditions.

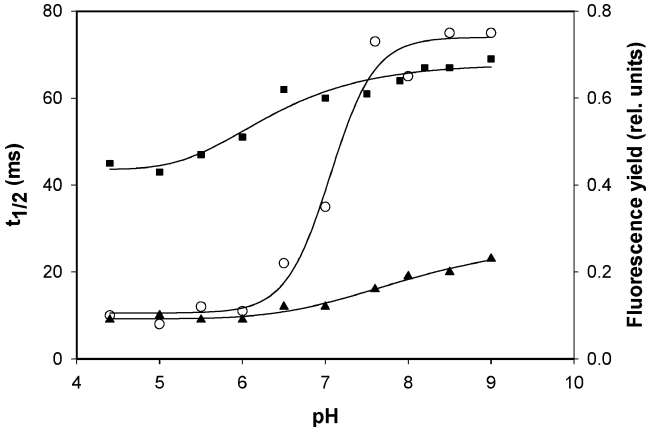

FIGURE 2: pH dependence of the maximum fluorescence yield (F_{max}) following flash excitation (■), the final fluorescence yield (F_{fin}) detected after decay of the flash-induced yield from the F_{max} level (▲), and the apparent half-time ($t_{1/2}$) for fluorescence decay (○). At least three sets of decay kinetics were averaged for the determination of each data point. See the legend of Figure 1 and the text for other experimental details.

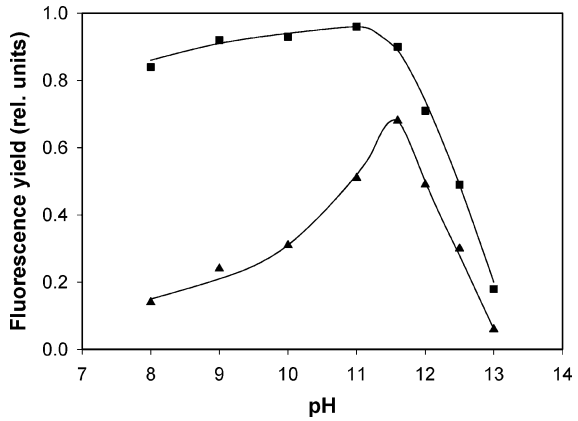

FIGURE 3: pH dependence of F_{max} (■) and F_{fin} (▲) in PSII(−Mn) membranes at alkaline pHs. The flash-probe fluorescence decay parameters were measured in the presence of 37.5 μM DCMU in 20 mM pyrophosphate buffer containing 0.4 M sucrose and 15 mM NaCl.

fluorescence decay half-time at higher pH ($t_{1/2}^{max}$) in Figure 2 is 75 ms, whereas the corresponding value found by Mamedov *et al.* (*24*) was 131 ms. The discrepancy might be due to the different strain of organisms used and/or the different temperature of the samples in the two experiments. In investigating the reason for this discrepancy, we determined that the apparent fluorescence decay $t_{1/2}$ at alkaline pHs (but not at acidic pHs) is quite dependent on the temperature of the sample. For example, at pH 9.0, it increases from 75 ms at 22 °C to ca. 300 ms at 7 °C (data not shown). Details about a temperature effect on the reduction of $Y_Z^{\bullet}$ are now being studied.

pH 8.0−13.0. The pH titration shown in Figure 2 did not enable us to estimate a pK_{app} for the kinetic parameter F_{fin}. However, the existence of a high fluorescent state that does not decay to the F_0 level has been observed previously at neutral pHs (*23*, *38*, *42*, *55*, *56*), and an increase in F_{fin} with pH up to pH 10.0 has also been reported by another group (*24*). On the other hand, Figure 3 shows the dependence of F_{max} and F_{fin} at pHs between 8 and 13.0 in pyrophosphate buffer. The F_{max} level changed little up to pH 11, and thereafter decreased to near zero with a pK_{app} of ∼12.5. This

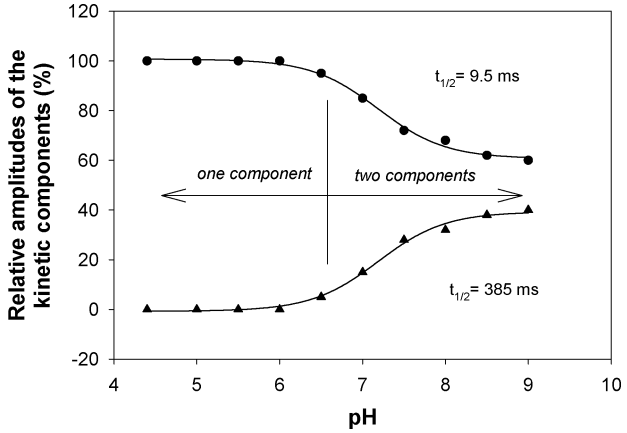

FIGURE 4: Relative amounts of the two exponentially decaying components deconvoluted from the flash-probe fluorescence yield kinetics in PSII(−Mn) membranes as a function of pH. The fast (●) and slow (▲) phases have $t_{1/2}$ values of 9.5 and 385 ms, respectively. The fluorescence decay at pH <6.0 can be fit with a single component ($t_{1/2}$ = 9.5 ms), while at pH >6.0, a second slower component with a $t_{1/2}$ of 385 ms is required.

pK_{app} is similar to that of arginine/arginate (12.5). One possible explanation for the drop in F_{max} at high pH is the deprotonation of an arginine residue that directly inhibits Q_a reduction. The reported involvement of arginines in maintaining electron transport capacity on the acceptor side of PSII (*57*, *58*) supports this suggestion. However, other reasons such as the inherent inability of PSII to perform charge sepsaration at such high pHs cannot be excluded. The value of F_{fin} in Figure 3 continued to increase with pH; the rate of increase accelerated at higher pHs, and F_{fin} reached a maximum at pH ∼11.5. At this point, the F_{fin} level was close to that of F_{max}, but then decreased in parallel with F_{max}. The pK_{app} of the ascending part of the F_{fin} curve equals 10.5, similar to the pK of the tyrosine/tyrosinate couple (10.3). Since donation of an electron by exogenous Mn(II) to PSII has a pK_{app} of 5.2 (*49*) and exhibits a very different pH profile, we can conclude that the observed pH dependence of F_{fin} is not due to electron donation by residual Mn [Tris treatment, like hydroxylamine, does not remove all Mn from PSII and leaves 0.1−0.8 Mn atom per RC of PSII (*59*)].

Deconvolution of the Fluorescence Decay Curves. The kinetics of charge recombination in PSII(−Mn) particles from *Synechocystis* sp. PCC6803 (*60*, *61*) or PSII-enriched membranes from spinach (*55*) can be represented as the sum of two (*55*) or three (*60*, *61*) exponential components at 315 and 325 nm (optical measurements of the Q_a^- decay kinetics). Optical measurements of $Y_Z^{\bullet}$ reduction at 292 and 287.5 nm have also been fitted with one (*55*) or two (*60*, *61*) exponentials. In Figure 4, we deconvolute the fluorescence decay kinetics measured at different pHs in spinach PSII membranes, assuming that the $t_{1/2}$ values of the individual exponential components do not change with pH (see the discussion in ref *62*). In support of this supposition, we point out that the rate constants for $P680^+$ reduction in Mn-depleted PSII particles vary only moderately with pH (*26*). Furthermore, Ahlbrink *et al.* (*4*) found that the rate of the fast kinetic component ($k_f = 7 \times 10^5\ s^{-1}$) in the reduction of $P680^+$ in Mn-depleted PSII core particles was nearly pH-independent, and the rate of the slow component ($k_s = 2-10 \times 10^4\ s^{-1}$) exhibited an only weak pH dependence. The fluorescence decay yield due to charge recombination,

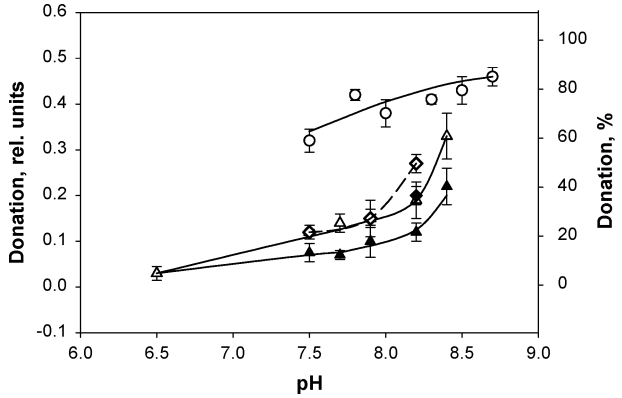

FIGURE 5: Effect of Tricine (50 mM Tricine, 0.4 mM sucrose, and 15 mM NaCl), HEPES (50 mM HEPES, 0.4 mM sucrose, and 15 mM NaCl), and MES (50 mM MES, 0.4 mM sucrose, and 15 mM NaCl) buffers on iron blocking at the HA_Z Mn-binding site in PSII(−Mn) membranes. The HA_Z site was blocked by incubating the membranes (25 μg of Chl/mL) in buffer A (pH 6.5) with 15 μM Fe(II) under room light for 2 min. The samples were then pelleted, resuspended in buffer at the indicated pHs, and incubated in the dark for an additional 5 min in Tricine (○), HEPES [(◇) 5 min incubation and (◆) 1.5 min incubation], or MES [(△) 5 min incubation and (▲) 1.5 min incubation] buffer. After incubation, the samples were again pelleted, but this time they were resuspended in buffer A at pH 6.5. The amount of unblocked HA_Z site, due to the release of bound iron cations from the membranes, was estimated from the amount of Mn(II) electron donation to $Y_Z^\bullet$ via the HA_Z site. The results were expressed as the relative amount of reducible $Y_Z^\bullet$ determined as $[(F_{max} - F_{fin})/F_{fin}]^{-Mn(II)} - [(F_{max} - F_{fin})/F_{fin}]^{+Mn(II)}$, where F_{max} and F_{fin} represent the maximum fluorescence level and the steady state fluorescence level after decay from F_{max} in the absence and presence of 10 μM Mn(II), respectively. As the scale, 0.55 relative unit equals 100% donation.

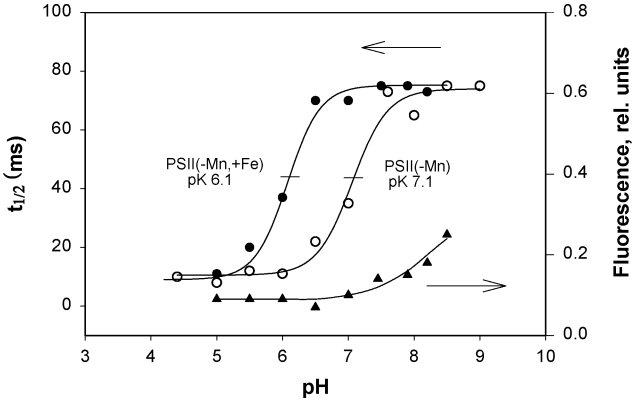

FIGURE 6: pH dependence of the flash-probe fluorescence parameters, apparent $t_{1/2}$ (●) and F_{fin} (▲), in PSII(−Mn) membranes with an iron-blocked HA_Z site [PSII(−Mn,+Fe)]. For comparison, the dependence of the $t_{1/2}$ in PSII(−Mn) membranes is also presented (○). The fluorescence measurements were taken after the iron-blocked samples were pelleted and resuspended in buffer at the indicated pHs.

measured at acidic pHs, can be fitted using only one exponential with a $t_{1/2}^f$ equivalent to the fast apparent $t_{1/2}$ (9.5 ms) reported in Figure 2. Above pH 6.0, the decay cannot be represented by a single-exponential component, and a second component ($t_{1/2}^s$) is necessary to fit the data. In this experiment, $t_{1/2}^s$ is significantly longer than $t_{1/2}^f$ and is equal to 385 ms. The amplitudes of the two individual components as a function of pH are shown in Figure 4. The amount of the fast component starts to decrease at pH >6.0, where the slow component starts to appear. The pK_{app} values of both components coincide with the pK_{app} of the $t_{1/2}$ of the species (base B) that controls electron transport to $Y_Z^\bullet$ (see Figure 2). These results imply that control of electron transport to $Y_Z^\bullet$ is determined by a single species in Mn-depleted PSII membranes. When this species becomes deprotonated, the rate of back electron transport between $Y_Z^\bullet$ and P680 decreases significantly.

pH Dependence of the Fluorescence Decay in Mn-Depleted PSII Membranes with an Fe-Blocked HA_Z Mn-Binding Site

pH 4.4−8.4. It is known that alkaline pH destabilizes the tetranuclear Mn cluster in the OEC and thus might also affect iron bound to the same site. Consequently, before investigating the effect of pH on PSII(−Mn,+Fe) membranes, we studied the stability of the blocking iron at alkaline pHs. The blocked membranes were incubated for 5 min in Tricine, or for 1.5 and 5 min in HEPES and MES buffers at the pHs indicated in Figure 5, and subsequently, electron donation by Mn(II) to $Y_Z^\bullet$ was assessed in buffer A at pH 6.5. Extraction of any specifically bound iron should be accompanied by an unblocking of the HA_Z site and the appearance of Mn(II) donation to $Y_Z^\bullet$ (*49*). The data obtained in Figure 5 show that incubation of the blocked PSII membranes in Tricine leads to extensive extraction of bound iron at all pHs that were tested (7.5−8.7). At pH >8.0, incubation of PSII(−Mn,+Fe) membranes in either HEPES or MES leads to the partial extraction of the bound iron as detected by the ability of the HA_Z site to accept electrons from Mn(II). The MES effect is weaker than the HEPES effect at pH >8.0, and the amount of iron extracted is dependent on the incubation time. As a consequence of these controls, we used only MES buffer to examine the effect of a pH of ≤8.2 on the fluorescence decay profiles in these same membranes.

In preliminary studies (*49*), we observed that blocking the HA_Z site with iron increased the apparent $t_{1/2}$ of the flash-probe fluorescence decay from 22 to 70 ms when the measurements were carried out at pH 6.5. However, as seen in Figure 6, the shift in the apparent $t_{1/2}$ occurs over only a narrow pH range. At pH <5.0, the fluorescence decay kinetics ($t_{1/2} \sim 9$ ms) do not change after the HA_Z site is blocked with iron. The same situation occurs at pH >8.0, where the apparent $t_{1/2}$ was the same for PSII(−Mn) membranes with or without an Fe-blocked HA_Z site. However, between pH 5.5 and 8.0, there is a considerable shift in the pK_{app} (from 7.1 to 6.1) of the component that controls electron transfer to Y_Z. Thus, the binding of iron cation(s) to the HA_Z Mn-binding site changes only the pK_{app} of the component forming the hydrogen bond with Y_Z. The effect of pH on F_{fin} did not change when the HA_Z site was blocked with iron (compare Figures 2 and 6) over the pH range that was investigated. As pointed out above, the pH titration of F_{fin} and F_{max} at pH >8.2 could not be done due to the effect of alkaline pH on the bound iron. If the flash-probe fluorescence decay profiles of PSII(−Mn,+Fe) membranes are deconvoluted using $t_{1/2}$ values of 9.5 and 385 ms as in Figure 4, the behavior of the two exponentials as a function of pH is the same as that of samples with an unblocked HA_Z site, except that the pK_{app} values of the slow and fast components are shifted to a pH of 6.1 (compare Figures 4 and 7).

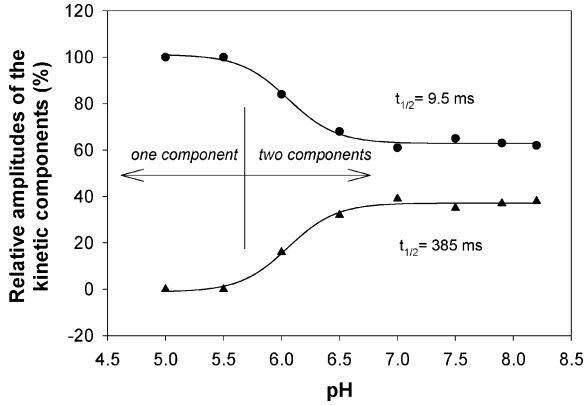

FIGURE 7: Relative amplitudes of the two exponentially decaying components deconvoluted from the flash-probe fluorescence yield kinetics in PSII(−Mn,+Fe) membranes as a function of pH. The fast (●) and slow (▲) phases have lifetimes of 9.5 and 385 ms, respectively. The fluorescence decay kinetics at pH <5.5 can be described by a single component ($t_{1/2}$ = 9.5 ms), while at pH >5.5 the second, slow component appears.

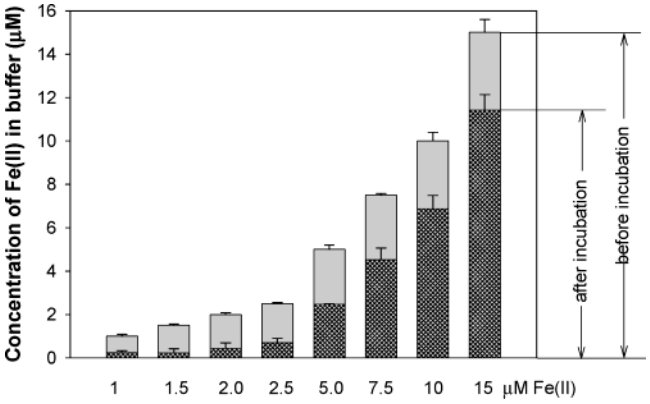

FIGURE 8: Concentration of Fe(II) in buffer A before and after incubation of PSII(−Mn) membranes (25 μg of Chl/mL) for 2 min with ferrous iron under weak light. The concentration of Fe(II) in solution after incubation with PSII(−Mn) membranes was measured in the supernatant immediately after removal of the membranes by centrifugation. The numbers at the bottom of the figure are the concentrations of Fe(II) added to the incubation buffer.

Table 1: Mössbauer Parameters for ^{57}Fe Cations Detected in PSII(−Mn) Membranes after Incubation of Membranes with either ^{57}Fe(II) or ^{57}Fe(III)[a]

sample	isomer shift δ (mm/s)	quadrupole splitting ΔE_Q (mm/s)
Mn-depleted PSII membranes with ^{57}Fe(II)	0.51	0.65
Mn-depleted PSII membranes with ^{57}Fe(III)	0.49	0.75

[a] See the text for experimental details.

Number of Iron Cations Required To Block the HA_Z Mn Site. A previous study (*49*) reported some of the properties of the blocking process, including the Fe concentration, the exposure time, and pH dependences. We have now attempted to place an upper limit on the number of iron cations binding to the HA_Z site by determining the number of cations that must be oxidized to achieve the blocking effect. To do this, we measured the concentration of Fe(II) remaining in solution after incubating Mn-depleted PSII membranes with Fe(II).

There are two possible reasons for the disappearance of ferrous cations from the solution during incubation, oxidation of Fe(II) cations or ligation of Fe(II) to the sample membrane. We eliminated the latter possibility using Mössbauer spectroscopy. Mn-depleted PSII membranes were incubated in the light with $^{57}FeSO_4$ under conditions providing the maximal blocking effect but minimizing the amount of nonspecifically bound iron cations (see Materials and Methods for details). The 80 K Mössbauer spectrum of PSII(−Mn,+Fe) membranes exhibits one doublet with the spectroscopic parameters typical of Fe(III) and shown in Table 1. A doublet typical of the high-spin ferrous state [quadrupole splitting (ΔE_Q) of around 3 mm/s and isomer shift (δ) of 1.1−1.3 mm/s] (*63*−*65*) was not observed in the spectrum. The relatively large absorption of the sample (5%), incubated with ^{57}Fe(II) in this experiment, makes it improbable that a significant amount of Fe(II) doublet could have been overlooked in the spectra. Furthermore, the Mössbauer spectrum of Mn-depleted PSII membranes incubated with ^{57}Fe(III) cations shows a quadrupole doublet with similar parameters (Table 1). These data indicate that PSII(−Mn) membranes incubated with ferrous cations in fact contain only ferric cations after illumination and that no Fe(II) is bound to the membranes. Although the spectra of samples with or without a blocked HA_Z Mn-binding site are similar at 80 K, they have different forms at 5 K (data not shown); however, conclusions about the structure of the specifically bound iron complex are premature at this point.

Figure 8 shows the concentration of Fe(II) remaining in solution after Mn-depleted PSII membranes have been incubated with different amounts of Fe(II) under cool white light (4 μE m^{-2} s^{-1}, PAR) for 2 min. The data indicate that (a) the extent of iron oxidation increases with the initial concentration of Fe(II) in the buffer, (b) saturation of iron oxidation takes place at Fe(II) concentrations of >5 μM, and (c) at 2 μM, the lowest concentration of Fe(II) that totally blocks the HA_Z site under our conditions (*49*), the amount of Fe(II) still remaining in the buffer after incubation was ∼20%. This means that blocking occurs when ∼14 Fe cations/RC are oxidized (calculated on the basis of 220 Chls per RC).

This number seems rather large, but we must consider that there are several ways for Fe(II) to be oxidized in our samples. In fact, only light-dependent Fe(II) oxidation via the HA_Z site causes the blocking effect. We can exclude Fe(II) oxidation by oxygen in the buffer; only 5% of the iron can be oxidized in buffer A at pH 6.5 over an incubation period of 1 h, which is much longer than the 2 min it takes to form the Fe block (*49*). This means that the primary routes for iron oxidation are associated with the Mn-depleted PSII membranes themselves. It is known that PSII(−Mn) membranes have two sites for the oxidation of exogenous electron donors such as Mn(II), DPC, and I^- (*66*), one involving high-affinity and the other low-affinity donation. The high-affinity oxidation site includes $Y_Z^\bullet$ as the oxidant, while the nature of the oxidant at the low-affinity site is not clear. Fe(II) can also be oxidized at high- and low-affinity sites. This is clearly seen in Figure 9, where oxidation of exogenous Fe(II) is shown to occur at concentrations above 2 μM, where the oxidation of Fe(II) via $Y_Z^\bullet$ is blocked (*49*), and thus must occur through the low-affinity site. The concentration dependence of Fe(II) oxidation in Figure 9 is unusual in the 0−0.5 μM Fe(II) range, where the rate of iron oxidation seems to increase linearly with Fe(II) concentration [but this

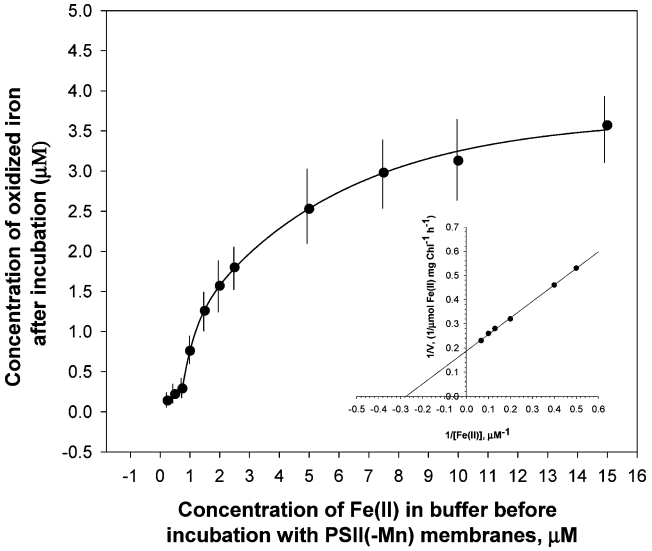

FIGURE 9: Amount of Fe(II) oxidized by Mn-depleted PSII membranes during a 2 min incubation under weak light as a function of added ferrous iron. See the Figure 5 legend and text for other experimental details. The inset shows a Lineweaver−Burk plot of the data presented in the main panel at iron concentrations of ≥2 μM.

range is close to the ±0.1 μM Fe(II) accuracy of the measurements]. However, above this range, the shape of the curve resembles those of the curves obtained for the oxidation of other exogenous electron donors (*66*). The inset of Figure 9 is a Lineweaver−Burk plot of the data above 2 μM Fe(II) and shows that there is only one low-affinity site for iron oxidation. This site has a K_m of 3.6 μM and a V_{max} of 5.3 μmol of Fe(II) (mg of Chl)$^{-1}$ h^{-1}. Using these parameters, the rate of Fe(II) oxidation via the low-affinity site can be determined at any concentration of added ferrous iron using the equation

$$V = \frac{V_{max}[S]}{K_m + [S]}$$

where [S] is the Fe(II) concentration.

For the above equation to be valid, the concentration of the substrate should be significantly larger than 2 μM to neglect the amount of Fe(II) cations oxidized via the high-affinity site. We chose 10 μM because the time dependence of the blocking effect was determined for this concentration (40 s) (*49*). Using the estimated K_m and V_{max} values, we can calculate that the number of iron cations oxidized via the low-affinity site during the blocking process was equal to 9.5 iron cations/RC. Subtracting this from the 14 Fe cations/RC oxidized by PSII(−Mn) membranes during the blocking procedure yields 4.5 ± 0.9 iron cations oxidized/RC by the HA_Z site.

DISCUSSION

Fluorescence Measurements. The rate of fluorescence decay in the absence of the Mn cluster depends on the recombination rate of $Y_Z^{\bullet}P680PheoQ_a^-$. The recombination is thought to take place initially between Q_a^- and $P680^+$ [$t_{1/2}$ = 100−200 μs (*67*, *68*)] and depends on the population of $P680^+$. The population of $P680^+$, in turn, is determined by the $Y_ZP680^+ \leftrightarrow Y_Z^{\bullet}P680$ equilibrium, which is governed by the equilibrium constant K_{ZP} (=$[Y_Z^{\bullet}P680]/[Y_ZP680^+]$) (*19*). Since the recombination time between Q_a^- and $Y_Z^{\bullet}$, determined by the flash-probe fluorescence method, is much larger than that between Q_a^- and $P680^+$ [i.e., the former is several tens of milliseconds (*24*, *37*, *38*, *42*)], the kinetics of fluorescence decay must be determined mainly by the concentration of $P680^+$, which we saw depends on the rate of back electron transport from P680 to $Y_Z^{\bullet}$.

Table 2: Half-Times for $Y_Z^{\bullet}$ Reduction in Mn-Depleted PSII Materials

pH	method	$t_{1/2}$ (ms)	sample	ref
6.0	EPR	9	PSII membranes, spinach	*71*
	flash-probe fluorescence	9	PSII membranes, spinach	this study
6.5	EPR	40	PSII membranes, spinach	*42*
	flash-probe fluorescence	25	PSII membranes, spinach	*42*
	flash-probe fluorescence	22	PSII membranes, spinach	this study
7.5	optical	107	PSII membranes, spinach	*55*
	flash-probe fluorescence	73	*C. reinhardtii* thylakoids	*24*
	flash-probe fluorescence	72	BBY membranes, spinach	this study
9.0	EPR	110	*C. reinhardtii* thylakoids	*24*
	flash-probe fluorescence	131	*C. reinhardtii* thylakoids	*24*
	flash-probe fluorescence	75	PSII membranes, spinach	this study[a]

[a] The differences in temperatures used for the different measurements can account for the lower value of $t_{1/2}$. The temperature differences are more pronounced at higher pHs (see the Results).

Nevertheless, the relationship between the Q_a^- population and the fluorescent yield can be nonlinear due to energy transfer between PSII units (*69*). To minimize the nonlinearity in the experiments described in the Results, we removed all divalent cations from the assay buffer. The results of Melis and Homann (*70*) and those compiled in Table 2 indicate that under such conditions the exitonic connectivity between PSII units in Mn-depleted spinach PSII membranes is small. Table 2 compares the $t_{1/2}$ values for $Y_Z^{\bullet}Q_a^-$ recombination found in our experiments using the flash-probe fluorescence method with $t_{1/2}$ values for $Y_Z^{\bullet}$ reduction kinetics determined both by EPR (*24*, *42*, *71*) and by optical measurements of the absorption changes at 292 nm (*55*). Table 2 also shows that there is no pH dependence of the exitonic connectivity between PSII units in the absence of divalent cations.

Kinetic Parameter F_{fin}. In our experiments, we found that increasing the pH of the buffer increased F_{fin}, which reflects the fraction of $Y_Z^{\bullet}$ not involved in the recombination process. Others have attributed F_{fin} to the action of an unknown donor (*23*, *24*, *55*, *56*). Possible alternative electron donors to $P680^+$ are Y_D, cytochrome b_{559}, and residual Mn. Mamedov *et al.* (*24*) excluded Y_D, due to the lack of inducible Y_D oxidation in their experimental preparations (which show substantial F_{fin}). Cytochrome b_{559} was also excluded as a potential $P680^+$ donor by Rappaport and Laverne (*55*), based on the lack of specific spectroscopic changes. Our pH titration of F_{fin} (Figures 2 and 3) now excludes residual Mn(II), since the shape of the F_{fin} curve is different from that of donation of an electron by Mn(II) to PSII(−Mn) membranes (*49*). It is still possible that other alternative donors reduce $Y_Z^{\bullet}$ under these conditions (but, see refs *24* and *55*). However, Figure 3 shows that F_{fin} has a pK_{app} of 10.5, which corresponds to the p*K* of the tyrosinate/tyrosine couple in solution (10.3).

This result supports the pK_{app} value of 10.3 reported by Hays *et al*. (*26*) in experiments with D1-H190 mutants. On the basis of these results, we suggest that the increase of F_{fin} with pH is governed not by the action of an unknown donor such as Mn(II) but by the deprotonation of Y_Z itself. Since the reduction of $Y_Z^{\bullet}$ is also a proton-coupled process and requires reprotonation (see refs *27*, *28*, and *62*), the process should be retarded at pHs above the pK_{app} of Y_Z, and this is indeed the case (Figure 3). Possibly, the acceleration of the forward reaction (the reduction of $P680^+$ by Y_Z) at high pHs is determined in part by the deprotonation of tyrosine itself. Thus, on the basis of our data, we suggest that the changes in the rate of electron transport between Y_Z and P680 with pH in the pH range of 6.0−8.0 are determined by the deprotonation and/or reprotonation of base B, the hydrogen bond partner to Y_Z, whereas Y_Z itself has a significantly higher pK_{app} (10.3).

Kinetic Components of Charge Recombination. Deconvolution of the recombination kinetics was carried out assuming that the rate constants associated with the process are independent of pH. This in turn assumes that the proton equilibria are slow with respect to observed rates of electron transfer, and that pH changes affect only the relative contributions of each exponential component. This assumption was also used by Ahlbrink *et al*. (*4*) and Hays *et al*. (*26*) (although see refs *19* and *30*) in the deconvolution of their data. Our fitted data (Figure 4) show that the reduction of $Y_Z^{\bullet}$ is controlled by only one hydrogen bond acceptor, which forms a hydrogen bond with a tyrosine. This result is consistent with the data of Kühne and Brudvig (*72*), who showed that only one proton participates in the rate-limiting step. However, according to the data in Figure 4, the formation of a hydrogen bond at alkaline pHs involves only a fraction (∼40%) of the Y_Z pool. This situation hampers our ability to determine accurately the p*K* of the hydrogen bond partner for Y_Z since the sigmoidal curve characteristic of the deprotonation process does not reach 100% at alkaline pHs. Therefore, the p*K* values determined from the results presented in Figures 4 and 7 can be considered only apparent p*K* values, as were the pK_{app} values determined from curves in Figures 2 and 6. As a consequence, we can use the pK_{app} values determined in our study as only a comparative parameter for investigating the global effects of iron blocking on charge recombination in PSII(−Mn) membranes.

Iron Blocking. Significant modification of the donor side properties of PSII occur upon the extraction of Mn. These include the increased accessibility of Y_Z to exogenous electron donors and the lowered rate of electron transfer from Y_Z to $P680^+$ (*4*, *19*, *25*, *26*, *29*−*31*). Several models have been proposed to explain these changes in the properties following Mn depletion. According to Debus and co-workers (*26*, *28*), the decrease in the rate of Y_Z oxidation is caused by the disruption of a hydrogen bond between Y_Z and D1-H190 (*26*), and proton transfer between Y_Z and D1-H190 occurs via hydrogen bonds formed by at least two water molecules that transiently connect Y_Z and D1-H190. However, FTIR measurement did not reveal significant perturbations in the immediate environment of the $Y_Z^{\bullet}$ phenoxyl group after Mn depletion (*20*). According to Junge and co-workers (*4*, *73*), the rate of electron transfer from Y_Z to $P680^+$ is controlled by an amino acid residue called "base B". Hydrogen-bonded with base B, Y_Z exists as tyrosinate, and only the deprotonated state of Y_Z allows for rapid nanosecond electron transfer to $P680^+$. However, the pK_{app} of base B changes from a value of 4.5 in active, O_2-evolving material to a value of ∼7.0 in Mn-depleted PSII core preparations (*4*). This increase in pK_{app}, resulting from the extraction of the Mn cluster, leads to the protonation of base B and slows the rate of Y_Z oxidation (*4*). Our results show that blocking the HA_Z Mn-binding site with iron results in an appreciable shift of the Y_Z hydrogen bond partner pK_{app} to a lower pH. This is consistent with the suggestion of Junge and co-workers (*4*), although the value of the pK_{app} in blocked membranes is still significantly higher than the estimated pK_{app} (4.5) for electron transfer from Y_Z to $P680^+$ in intact PSII. This discrepancy can be attributed either to the difference between the coordination of iron and manganese ions by PSII or to an as yet unrecognized effect.

Decreases in the rate of the back reaction ($P680 \rightarrow Y_Z^{\bullet}$) are accompanied by complementary increases in the rate of the forward reaction ($Y_Z \rightarrow P680^+$) (refs *19*, *24*−*26*, *55*, and *74* and our results). Thus, one would predict that blocking the HA_Z site might be accompanied by an acceleration of Y_Z oxidation (or $P680^+$ reduction), corresponding to the restoration (at least partially) of the rate of electron transfer disrupted by Mn depletion. However, the effects of several metal cations (Co^{2+}, Zn^{2+}, Fe^{2+}, Fe^{3+}, Mn^{2+}, Ca^{2+}, and Mg^{2+}) on the rate of $P680^+$ reduction were measured recently (*74*). All these cations with the exception of Ca^{2+} and Mg^{2+} decreased the rate of $P680^+$ reduction. Since Fe(II) decreased rather than increased the rate of electron transfer from Y_Z to $P680^+$, we note that the Fe(II) in that study (*74*) was added just prior to the measurements. Under those conditons, blocking of the HA_Z site could not have occurred, because preincubation of Mn-depleted PSII core particles with Fe(II) for the length of time under weak light, necessary for blocking (*49*), did not occur. Nevertheless, some of the results from that work (*74*) support our suggestion that the decrease in the $Y_Z^{\bullet}$ reduction rate by iron blocking should be accompanied by an increase in the Y_Z oxidation ($P680^+$ reduction) rate. Ahlbrink *et al*. (*74*) found that addition of Ca^{2+} and Mg^{2+} separately accelerated the reduction of $P680^+$, shifting the apparent pK_{app} of base B from 7.4 to ∼6.7. Indeed, we observed a complementary effect of these cations in our flash-probe fluorescence experiments, where Ca^{2+} and Mg^{2+} decreased the rate of $Y_Z^{\bullet}$ reduction (unpublished results).

Iron Stoichiometry. The number of iron cations that must be oxidized at the HA_Z site to induce the blocking effect is between four and five (Figures 8 and 9). However, we cannot say that this range reflects the number of iron cations actually bound at the HA_Z site. Nevertheless, this number is close to the four Mn ions forming the Mn cluster as well as the number of metal ions (Mn + Ca) forming the OEC (five). Moreover, insertion of the diiron cluster into the ribonucleotide reductase apoenzyme, which has the same diiron-binding motifs found on the carboxyl ends the of PSII D1 and D1 polypeptides (*48*), requires at least six irons, of which four Fe(II) cations per enzyme are oxidized (*75*).

Blocking itself is a light-driven process where ferrous cations must be oxidized to block the HA_Z Mn-binding site (*49*). Despite the number of iron cations oxidized during the process, blocking occurs in the absence of an added exogenous electron acceptor. This is not surprising, because

it is well-known that photoactivation (self-assembly of the Mn cluster) can also occur in the absence of an exogenous electron acceptor (*76*). Oxygen most likely serves as the electron acceptor for both photoactivation and Fe blocking since the reduction of O_2 on the acceptor side of PSII is well-known (*77*, *78*).

Summary. In conclusion, we have observed that the presence of iron bound to the HA_Z site causes a shift in the pK_{app} for $Y_Z^\bullet$ reduction from 7.1 to 6.1, without affecting the rate of $Y_Z^\bullet$ reduction at acidic or alkaline pHs. These results suggest that the extraction of Mn from the OEC, rather than disrupting the hydrogen bond between base B and Y_Z, in fact shifts the pK_{app} of base B, supporting the work of Ahlbrink *et al*. (*4*). Furthermore, the coordination of iron cation(s) at the HA_Z Mn-binding site provides for significant changes in the protein matrix around Y_Z. Bound iron cations prevent the access of Y_Z for most exogenous donors (*49*) and shift the pK_{app} of base B controlling the rate of electron transfer between P680 and $Y_Z^\bullet$. These results show that bound iron cations can partially restore some of the structural organization on the donor side of PSII disrupted by extraction of the tetrameric Mn cluster.

ACKNOWLEDGMENT

We thank Professor A. B. Rubin for his continued support of this work at the National Renewable Energy Laboratory, Prof. F. Parak for his helpful suggestions on the Mössbauer studies, Dr. M. Reiner for taking the Mössbauer measurements, and Dr. Maria L. Ghirardi for many useful discussions as well as her critical reading of the manuscript.

REFERENCES

1. Barber, J., and Archer, M. D. (2001) P680, the primary electron donor of photosystem II, *J. Photochem. Photobiol., A 142*, 97−106.
2. Brettel, K., Schlodder, E., and Witt, H. T. (1984) Nanosecond reduction kinetics of photooxidized chlorophyll-a_{II} (P-680) in single flashes as a probe for the electron pathway, H^+-release and charge accumulation in the O_2-evolving complex, *Biochim. Biophys. Acta 766*, 403−415.
3. Schlodder, E., Brettel, K., Schatz, G. H., and Witt, H. T. (1984) Analysis of the Chl-a^+_{II} reduction kinetics with nanosecond time resolution in oxygen-evolving photosystem II particles from *Synechococcus* at 680 and 824 nm, *Biochim. Biophys. Acta 765*, 178−185.
4. Ahlbrink, R., Haumann, M., Cherepanov, D., Bögershausen, O., Mulkidjanian, A., and Junge, W. (1998) Function of tyrosin Z in water oxidation by photosystem II: electrostatical promotor instead of hydrogen abstractor, *Biochemistry 37*, 1131−1142.
5. Barry, B. A., and Babcock, G. T. (1987) Tyrosine radicals are involved in the photosynthetic oxygen-evolving system, *Proc. Natl. Acad. Sci. U.S.A. 84*, 7099−7103.
6. Tommos, C., Tang, X.-S., Warncke, K., Hoganson, C. W., Styring, S., McCracken, J., Diner, B. A., and Babcock, G. T. (1995) Spin-density distribution, conformation, and hydrogen bonding of the redox-active tyrosine Y_Z in photosystem II from multiple-electron magnetic-resonance spectroscopies: implications for photosynthetic oxygen evolution, *J. Am. Chem. Soc. 117*, 10325−10335.
7. Force, D. A., Randall, D. W., Britt, R. D., Tang, X.-S., and Diner, B. A. (1995) ^{2}H ESE-ENDOR study of hydrogen bonding to the tyrosine radicals $Y_D^\bullet$ and $Y_Z^\bullet$ of photosystem II, *J. Am. Chem. Soc. 117*, 12643−12644.
8. Tommos, C., Hoganson, C. W., Di Valentin, M., Lydakis-Simantiris, N., Dorlet, P., Westphal, K., Chu, H.-A., McCracken, J., and Babcock, G. T. (1998) Manganese and tyrosyl radical function in photosynthetic oxygen evolution, *Curr. Opin. Chem. Biol. 2*, 244−252.
9. Peloquin, J. M., Campbell, K. A., and Britt, R. D. (1998) ^{55}Mn Pulsed ENDOR demonstrates that the photosystem II "split" EPR signal arises from a magnetically-coupled mangano-tyrosyl complex, *J. Am. Chem. Soc. 120*, 6840−6841.
10. Zouni, A., Witt, H.-T., Kern, J., Fromme, P., Krauss, N., Saenger, W., and Orth, P. (2001) Crystal structure of photosystem II from *Synechococcus elongatus* at 3.8 Å resolution, *Nature 409*, 739−743.
11. Lakshmi, K. V., Eaton, S. S., Eaton, G. R., Frank, H. A., and Brudwig, G. W. (1998) Analysis of dipolar and exchange interactions between manganese and tyrosine Z in the $S_2Y_Z^\bullet$ state of acetate-inhibited photosystem II via EPR spectral simulations at X- and Q-bands, *J. Phys. Chem. B 102*, 8327−8335.
12. Limburg, J., Szalai, V. A., and Brudvig, G. W. (1999) A mechanistic and structural model for the formation and reactivity of a Mn−V═O species in photosynthetic water oxidation, *J. Chem. Soc., Dalton Trans*., 1353−1361.
13. Britt, R. D., Peloquin, J. M., and Campbell, K. A. (2000) Pulsed and parallel-polarization EPR characterization of the photosystem II oxygen-evolving complex, *Annu. Rev. Biophys. Biomol. Struct. 29*, 463−495.
14. Gilchrist, M. L., Ball, J. A., Randall, D. W., and Britt, R. D. (1995) Proximity of the Maganese Cluster of Photosystem II to the Redox-Active Tyrosine Y_z, *Proc. Natl. Acad. Sci. U.S.A. 92*, 9545−9549.
15. Hoganson, C. W., Lydakis-Symantiris, N., Tang, X.-S., Tommos, C., Warncke, K., Babcock, G. T., Diner, B. A., McCracken, J., and Styring, S. (1995) A hydrogen-atom abstraction model for the function of Y−Z in photosynthetic oxygen evolution, *Photosynth. Res. 46*, 177−184.
16. Thommos, C., and Babcock, G. T. (2000) Proton and hydrogen currents in photosynthetic water oxidation, *Biochim. Biophys. Acta 1458*, 199−219.
17. Candeias, L. P., Turconi, S., and Nugent, J. H. A. (1998) Tyrosine Y_Z and Y_D of photosystem II: Comparison of optical spectra to those of tyrosine oxidised by pulsed radiolysis, *Biochim. Biophys. Acta 1363*, 1−5.
18. Tang, X.-S., Zheng, M., Chisholm, D. A., Dismukes, G. C., and Diner, B. A. (1996) Investigation of the differences in the local protein environments surrounding tyrosine radicals $Y_Z^\bullet$ and $Y_D^\bullet$ in photosystem II using wild-type and the D2-Tyr160Phe mutant of *Synechocystis* 6803, *Biochemistry 35*, 1475−1484.
19. Diner, B. A., Force, D. A., Randall, D. W., and Britt, R. D. (1998) Hydrogen Bonding, Solvent Exchange, and Coupled Proton and Electron Transfer in the Oxidation and Reduction of Redox-Active Tyrosine Y_Z in Mn-Depleted Core Complexes of Photosystem II, *Biochemistry 37*, 17931−17943.
20. Berthomieu, C., Hienerwadel, R., Boussac, A., Breton, J., and Diner, B. A. (1998) Hydrogen Bonding of redox-active tyrosine Z of photosystem II probed by FTIR difference spectroscopy, *Biochemistry 37*, 10547−10554.
21. Svensson, B., Vass, I., Cedergren, E., and Styring, S. (1990) Structure of donor side components in photosystem II predicted by computer modelling, *EMBO J. 9*, 2051−2059.
22. Svensson, B., Etchebest, C., Tuffery, P., van Kan, P., Smith, J., and Styring, S. (1996) A model for the photosystem II reaction center core including the structure of the primary donor P_{680}, *Biochemistry 35*, 14486−14502.
23. Roffey, R. A., Kramer, D. M., Govindjee, and Sayre, R. T. (1994) Lumenal side histidine mutations in the D1 protein of photosystem II affect donor side electron transfer in *Chlamydomonas reinhardtii*, *Biochim. Biophys. Acta 1185*, 257−270.
24. Mamedov, F., Sayre, R. T., and Sryring, S. (1998) Involvement of histidine 190 on the D1 protein in electron/proton transfer reactions on the donor side of photosystem II, *Biochemistry 37*, 14245−14256.
25. Hays, A.-M. A., Vassiliev, I. R., Golbeck, J. H., and Debus, R. J. (1998) Role of D1-His190 in proton-coupled electron transfer reactions in photosystem II: a chemical complementation study, *Biochemistry 37*, 11352−11365.
26. Hays, A.-M. A., Vassiliev, I. R., Golbeck, J. H., and Debus, R. J. (1999) Role of D1-His190 in the proton-coupled oxidation of tyrosine Y_Z in manganese-depleted photosystem II, *Biochemistry 38*, 11851−11865.
27. Diner, B. A. (2001) Amino acid residues involved in the coordination and assembly of the manganese cluster of photosystem II. Proton-coupled electron transport of the redox-active tyrosines and its relationship to water oxidation, *Biochim. Biophys. Acta 1503*, 147−163.
28. Debus, R. J. (2001) Amino acid residues that modulate the properties of tyrosine Y_Z and the manganese cluster in the water

oxidizing complex of photosystem II, *Biochim. Biophys. Acta 1503*, 164−186.
29. Chroni, S., and Ghanotakis, D. F. (2001) Accessibility of tyrosine $Y^{\bullet}_Z$ to exogenous reductants and Mn^{2+} in various photosystem II preparations, *Biochim. Biophys. Acta 1504*, 432−437.
30. Conjeaud, H., and Mathis, P. (1980) The effect of pH on the reduction kinetics of *P*-680 in tris-treated chloroplasts, *Biochim. Biophys. Acta 590*, 353−359.
31. Christen, G., Karge, M., Eckert, H.-J., and Renger, G. (1997) The role of protonation steps in electron transfer reactions in Tris-treated photosystem 2 membrane, *Photosynthetica 33*, 529−539.
32. Nixon, P. J., and Diner, B. A. (1992) Aspartate 170 of the photosystem II reaction center polypeptide D1 is involved in the assembly of the oxygen-evolving manganese cluster, *Biochemistry 31*, 942−948.
33. Seibert, M., Tamura, N., and Inoue, Y. (1989) Lack of photoactivation capacity in *Scenedesmus obliquus* LF-1 results from loss of half the high-affinity manganese-binding site. Relationship to the unprocessed D1 protein, *Biochim. Biophys. Acta 974*, 185−191.
34. Ananyev, G. M., Murphy, A., Abe, Y., and Dismukes, G. C. (1999) Remarkable affinity and selectivity for Cs^+ and uranyl (UO_2^{2+}) binding to the manganese site of the apo-water oxidation complex of photosystem II, *Biochemistry 38*, 7200−7209.
35. Preston, C., and Seibert, M. (1991) The carboxyl modifier 1-ethyl-3-[3-(dimethylamino)propyl]carbodiimide (EDC) inhibits half of the high-affinity manganese-binding site in photosystem II membrane fragments, *Biochemistry 30*, 9615−9624.
36. Preston, C., and Seibert, M. (1991) Protease treatments of photosystem II membrane fragments reveal that these are four separate high-affinity manganese-binding site, *Biochemistry 30*, 9625−9633.
37. Diner, B. A., and Nixon, P. J. (1992) The rate of reduction of oxidized redox-active tyrosine, Z^+, by exogenous Mn^{2+} is slowed in a site-directed mutant, at aspartate 170 of polypeptide D1 of photosystem II, inactive for photosynthetic oxygen evolution, *Biochim. Biophys. Acta 1101*, 134−138.
38. Ghirardi, M. L., Lutton, T. W., and Seibert, M. (1996) Interactions between diphenylcarbazide, zinc, cobalt, and manganese on the oxidizing side of photosystem II, *Biochemistry 35*, 1820−1828.
39. Magnuson, A., and Andréasson, L.-E. (1997) Different manganese binding sites in photosystem II probed by selective chemical modification of histidyl and carboxylic acid residues, *Biochemistry 36*, 3254−3261.
40. Ghirardi, M. L., Lutton, T. W., and Seibert, M. (1998) Effects of carboxyl amino acid modification on the properties of the high-affinity, manganese-binding site in photosystem II, *Biochemistry 37*, 13559−13566.
41. Ghirardi, M. L., Preston, C., and Seibert, M. (1998) Use of a novel histidyl modifier to probe for residues on tris-treated photosystem II membrane fragments that may bind functional manganese, *Biochemistry 37*, 13567−13574.
42. Ono, T.-A., and Mino, H. (1999) Unique binding site for Mn^{2+} ion responsible for reducing an oxidized Y_Z tyrosine in manganese-depleted photosystem II membranes, *Biochemistry 38*, 8778−8785.
43. Campbell, K. A., Force, D. A., Nixon, P. J., Dole, F., Diner, B. A., and Britt, R. D. (2000) Dual-mode EPR detects the initial intermediate in photoassembly of the photosystem II Mn cluster: the influence of amino acid residue 170 of the D1 polypeptide on Mn coordination, *J. Am. Chem. Soc. 122*, 3754−3761.
44. Blubaugh, D. J., and Cheniae, G. M. (1992) Photoassembly of the photosystem II manganese cluster, in *Research in Photosynthesis* (Murata, N., Ed.) Vol. II, pp 361−364, Kluwer Academic Publishers, Dordrecht, The Netherlands.
45. Hsu, B.-D., Lee, J.-I., and Pan, R.-L. (1987) The high-affinity binding site for manganese on the oxidizing side of photosystem II, *Biochim. Biophys. Acta 890*, 89−96.
46. Semin, B. K., Ivanov, I. I., Rubin, A. B., and Parak, F. (1995) High-specific binding of Fe(II) at the Mn-binding site in Mn-depleted PSII membranes from spinach, *FEBS Lett. 375*, 223−226.
47. Semin, B. K., Davletschina, L., Ivanov, I. I., Reiner, M., and Parak, F. (1998) Formation of dinuclear Fe(III) center by interaction of Fe(II) with the Mn-binding site of Mn-deleted PSII membranes, in *Photosynthesis: Mechanism and Effects* (Garab, G., Ed.) Vol. II, pp 1415−1418, Kluwer Academic Publishers, Dordrecht, The Netherlands.
48. Semin, B. K., and Parak, F. (1997) Coordination sphere and structure of the Mn cluster of the oxygen-evolving complex in photosynthetic organisms, *FEBS Lett. 400*, 259−262.
49. Semin, B. K., Ghirardi, M. L., and Seibert, M. (2002) Blocking of electron donation by Mn(II) to $Y_Z^{\bullet}$ following incubation of Mn-depleted photosystem II membranes with Fe(II) in the light, *Biochemistry 41*, 5854−5864.
50. Porra, R. J., Tompson, W. A., and Kriedemann, P. E. (1989) Determination of Accurate Extinction Coefficients and Simultaneous-Equations for Assaying Chlorophyll-A and Chlorophyll-B Extracted with 4 Different Solvents: Verification of the Concentration of Chlorophyll Standards by Atomic-Absorption Spectroscopy, *Biochim. Biophys. Acta 975*, 384−394.
51. Philbrick, J. B., Diner, B. A., and Zilinskas, B. A. (1991) Construction and characterization of cyanobacterial mutants lacking the manganese-stabilizing polypeptide of photosystem II, *J. Biol. Chem. 266*, 13370−13376.
52. Nuijs, A. M., van Gorkom, H. J., Plijter, J. J., and Duysens, L. M. N. (1986) Primary-charge separation and excitation of chlorophyll *a* in photosystem II particles from spinach as studied by picosecond absorbance-difference spectroscopy, *Biochim. Biophys. Acta 848*, 167−175.
53. Butler, W. L. (1972) Primary nature of fluorescence yield changes associated with photosynthesis, *Proc. Natl. Acad. Sci. U.S.A. 69*, 3420−3422.
54. Robinson, H. H., and Crofts, A. R. (1983*)* Kinetics of the oxidation−reduction reactions of the photosystem II quinone acceptor complex, and the pathway for deactivation, *FEBS Lett. 153*, 221−226.
55. Rappaport, F., and Lavergne, J. (1997) Charge recombination and proton transfer in manganese-depleted photosystem II, *Biochemistry 36*, 15294−15302.
56. Chu, H.-A., Nguyen, A. P., and Debus, R. J. (1995) Amino acid residues that influence the binding of manganese or calcium to photosystem II. 1. The lumenal interhelical domains of the D1 polypeptide, *Biochemistry 34*, 5839−5858.
57. Xiong, J., Hutchison, R. S., Sayre, R. T., and Govindjee (1997) Modification of the photosystem II acceptor side function in a D1 mutant (arginine-269-glycine) of *Chlamydomonas reinhardti*, *Biochim. Biophys. Acta 1322*, 60−76.
58. Xiong, J., Minagawa, J., Crofts, A., and Govindjee (1998) Loss of inhibition by formate in newly constructed photosystem II D1 mutants, D1-R257E and D1-R257M, of *Chlamydomonas reinhardtii*, *Biochim. Biophys. Acta 1365*, 473−491.
59. Kuwabara, T., and Murata, N. (1983) Quantitative analysis of the inactivation of photosynthetic oxygen evolution and the release of polypeptides and manganese in the photosystem-II particles of spinach chloroplasts, *Plant Cell Physiol. 24*, 741−747.
60. Debus, R. J., Campbell, K. A., Peloquin, J. M., Pham, D. P., and Britt, R. D. (2000) Histidine 332 of the D1 polypeptide modulates the magnetic and redox properties of the manganese cluster and tyrosine Y_Z in photosystem II, *Biochemistry 39*, 470−478.
61. Debus, R. J., Campbell, K. A., Pham, D. P., Hays, A.-M. A., and Britt, R. D. (2000) Glutamate 189 of the D1 polypeptide modulates the magnetic and redox properties of the manganese cluster and tyrosine Y_Z in photosystem II, *Biochemistry 39*, 6275−6287.
62. Rappaport, F., and Lavergne, J. (2001) Coupling of electron and proton transfer in the photosynthetic water oxidase, *Biochim. Biophys. Acta 1503*, 246−259.
63. Garbes, A., Reifarth, F., Kurreck, J., Renger, G., and Parak, F. (1998) Correlation between protein flexibility and electron transfer from Q_a^- to Q_B in PSII membrane fragments from spinach, *Biochemistry 37*, 11399−11404.
64. Cadieux, E., Vrajmasu, V., Achim, C., Powlowski, J., and Münck, E. (2002) Biochemical, Mössbauer, and EPR studies of the diiron cluster of phenol hydroxylase from *Pseudomonas* sp. strain CF 600, *Biochemistry 41*, 10680−10691.
65. Semin, B. K., Davletshina, L. N., Novakova, A. A., Kiseleva, T. I., Lanchinskaya, V. Y., Aleksandrov, A. Y., Seifulina, N., Ivanov, I. I., Seibert, M., and Rubin, A. B. (2003) Accumulation of ferrous iron in *Chlamydomonas reinhardtii*. Influence of CO_2 and anaerobic induction of the reversible hydrogenase, *Plant Physiol. 131*, 1756−1764.
66. Blubaugh, D. J., and Cheniae, G. M. (1990) Kinetics of photoinhibition in hydroxylamine-extracted photosystem II membranes: relevance to photoactivation and sites of electron donation, *Biochemistry 29*, 5109−5118.
67. Haveman, J., and Mathis, P. (1976) Flash-induced absorption changes of the primary donor of photosystem II at 820 nm in

chloroplasts inhibited by low pH or tris-treatment, *Biochim. Biophys. Acta 440*, 346−355.
68. Renger, G., and Wolff, C. H. (1976) The existence of a high photochemical turnover rate at the reaction centers of system II in Tris-washed chloroplasts, *Biochim. Biophys. Acta 423*, 610−614.
69. Joliot, A., and Joliot, P. (1964) Kinetic study of the photochemical reaction liberating oxygen during photosynthesis, *C. R. Acad. Sci. Paris 258*, 4622−4625.
70. Melis, A., and Homann, P. H. (1978) A selective effect of Mg^{2+} on the photochemistry at one type of reaction center in photosystem II of chloroplasts, *Arch. Biochem. Biophys. 190*, 523−530.
71. Lydakis-Symantiris, N., Ghanotakis, D. F., and Babcock, G. T. (1997) Kinetic isotope effects on the reduction of the Y_z radical in oxygen evolving and tris-washed photosystem II membranes by time-resolved EPR, *Biochim. Biophys. Acta 1322*, 129−140.
72. Kühne, H., and Brudvig, G. W. (2002) Proton-coupled electron transfer involving tyrosine Z in photosystem II, *J. Phys. Chem. B 106*, 8189−8196.
73. Haumann, M., Mulkijanian, A., and Junge, W. (1999) Tyrosine-Z in oxygen-evolving photosystem II: a hydrogen-bonded tyrosinate, *Biochemistry 38*, 1258−1267.
74. Ahlbrink, R., Semin, B. K., Mulkidjanian, A., and Junge, W. (2001) Photosystem II of peas: effects of added divalent cations of Mn, Fe, Mg, and Ca on two kinetic components of $P680^+$ reduction in Mn-depleted core particles, *Biochim. Biophys. Acta 1506*, 117−126.
75. Pötsch, S., Lendzian, F., Ingemarson, R., Hörngerg, A., Thelander, L., Lubitz, W., Lassmann, G., and Gräslund, A. (1999) The iron−oxygen reconstitution reaction in protein R2-Tyr-177 mutants of mouse ribonucleotide reductase. EPR and electron nuclear double resonance studies on a new transiet tryptophan radical, *J. Biol. Chem. 274*, 17696−17704.
76. Tamura, N., and Cheniae, G. M. (1987) Photoactivation of the water-oxidizing complex in photosystem II membranes depleted of Mn and extrinsic proteins. I. Biochemical and kinetic characterization, *Biochim. Biophys. Acta 890*, 179−194.
77. Cleland, R. E., and Grace, S. C. (1999) Voltammetric detection of superoxide production by photosystem II, *FEBS Lett. 457*, 348−352.
78. Ivanov, B., and Khorobrykh, S. (2003) Participation of photosynthetic electron transport in production and scavenging of reactive oxygen species, *Antioxid. Redox Signaling 5*, 43−53.

BI036047P